

Quantum Circuit Transformation Based on Simulated Annealing and Heuristic Search

Xiangzhen Zhou^{1,2}, Sanjiang Li^{*2} and Yuan Feng^{†2}

¹State Key Lab of Millimeter Waves, Southeast University, Nanjing 211189, China

²Centre for Quantum Software and Information, Faculty of Engineering and Information Technology, University of Technology Sydney, NSW 2007, Australia

June 2019

Abstract

Quantum algorithm design usually assumes access to a perfect quantum computer with ideal properties like full connectivity, noise-freedom and arbitrarily long coherence time. In Noisy Intermediate-Scale Quantum (NISQ) devices, however, the number of qubits is highly limited and quantum operation error and qubit coherence are not negligible. Besides, the connectivity of physical qubits in a quantum processing unit (QPU) is also strictly constrained. Thereby, additional operations like SWAP gates have to be inserted to satisfy this constraint while preserving the functionality of the original circuit. This process is known as quantum circuit transformation. Adding additional gates will increase both the size and depth of a quantum circuit and therefore cause further decay of the performance of a quantum circuit. Thus it is crucial to minimize the number of added gates. In this paper, we propose an efficient method to solve this problem. We first choose by using simulated annealing an initial mapping which fits well with the input circuit and then, with the help of a heuristic cost function, stepwise apply the best selected SWAP gates until all quantum gates in the circuit can be executed. Our algorithm runs in time polynomial in all parameters including the size and the qubit number of the input circuit, and the qubit number in the QPU. Its space complexity is quadratic to the number of edges in the QPU. Experimental results on extensive realistic circuits confirm that the proposed method is efficient and can reduce by 57% on average the size of the output circuits when compared with the state-of-the-art algorithm on the most recent IBM quantum device viz. IBM Q20 (Tokyo).

1 Introduction

In Noisy Intermediate-Scale Quantum (NISQ) era, it is unrealistic to implement quantum error correction due to the strictly limited number of qubits [20]. This drawback brings huge challenge to quantum program compilation because the noise will have large impact on final circuits and may often make the results meaningless. Besides, the connectivity of qubits in an NISQ device is also limited. Only those neighbouring qubits can be coupled and only between them can two-qubit operations be implemented [24]. As a result, a large number of modifications must be done to adapt a quantum circuit to the real quantum devices. This process is termed as quantum circuit transformation [6], qubit mapping [13], qubit allocation [21], qubit routing [19] or qubit movement [15] in the literature. We call it quantum circuit transformation in this paper.

Quantum circuit transformation is an essential part for quantum circuit compilation. The main idea behind is to convert an ideal quantum circuit, in which full connectivity among qubits is assumed and noise is ignored, to a quantum circuit respecting constraints imposed by the NISQ devices [6]. Usually this process will bring in a large number of auxiliary gates like SWAP gates and Hadamard gates which will in turn increase both the size

*sanjiang.li@uts.edu.au

†yuan.feng@uts.edu.au

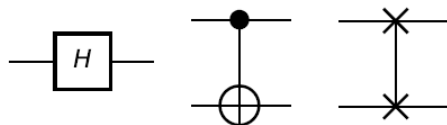


Figure 1: Hadamard, CNOT and SWAP gate (from left to right).

and depth of the generated quantum circuit and sometimes make the error of the whole circuit unacceptable [24]. Hence, it is vital for the success of quantum computation to find an automated approach that can efficiently transform any input quantum circuit into one that respects the physical constraints imposed by the NISQ devices with a small overhead in terms of the size, depth or error.

The quantum circuit transformation problem can be reduced to token swapping or template matching in graph theory [14, 2]. Unfortunately, both of these problems are NP-hard [6]. Hence, designing algorithms to solve the quantum circuit transformation problem while making trade off between time consuming and the quality of results has brought lots of interest in both the quantum computing community and the integrated circuits community [24].

There are currently three major approaches to the quantum circuit transformation problem. The first one is to use heuristic search to construct the output quantum circuit step by step from the original input quantum circuit [13, 19, 25, 21, 8]. Usually, these search algorithms need an initial mapping as the input, and it can be set arbitrarily or via some greedy methods [25, 19, 7]. Recently, a novel reverse traversal technique is proposed in [13] to choose the initial mapping with the consideration of the whole circuit. The second approach is to utilize unitary matrix decomposition algorithms to reconstruct a quantum circuit from scratch while preserving the functionality of the input circuit [16, 12]. The third one is to convert the quantum circuit transformation problem to some existing problems like AI planning and constraint programming and use ready-made tools for these problems to find acceptable results [4, 23].

In this paper, we follow the first approach. Our main contributions are listed as follows. First, we propose a simulated annealing based algorithm to find a near-optimal initial mapping for the input circuit. Second, we design a flexible heuristic cost function to evaluate the possible operations that may be applied to transform the current circuit. The heuristic function supports weight parameters to reflect the variable influence of gates in different layers. Third, a heuristic search algorithm with a novel selection mechanism is designed, where in each step of the search process, instead of selecting the operation with minimum cost to apply, we look one step ahead and select the operation which has the best consecutive operation to apply. In this way, the algorithm is able to avoid the local minimum effectively. Fourth, a pruning mechanism is introduced to reduce the size of search space and ensure the program terminates in reasonable time.

Note that the look-ahead mechanism has already been introduced in the heuristic cost function during the search process in existing works like [25, 13]. However, we adopt in this paper a double look-ahead mechanism: in addition to looking ahead at subsequent layers when defining the cost function, we also look ahead (at grandchild states) in finding the state with minimal cost in order to make the best transformation. Thanks to this novel idea, the proposed algorithm is able to find a better solution with less circuit size within acceptable running time. Experimental results on extensive realistic circuits show that our algorithm is efficient and, when compared with the state-of-the-art algorithms [25, 13], can reduce on average the size of the output circuits by above 10% on IBM QX5 and above 55% on IBM Q20.

The remainder of this paper is organized as follows: some background knowledge about quantum computation is given in Section 2, and the quantum circuit transformation problem is formally defined in Section 3. Section 4 is devoted to the detailed description of our proposed algorithm. We report experimental results in Section 5 and conclude the paper in Section 6.

2 Background

In classical computation, information is stored in memory in the form of binary digits, i.e., bits. The quantum counterpart of bit, called qubit, has two basis states denoted by $|0\rangle$ and $|1\rangle$, respectively. Different from a

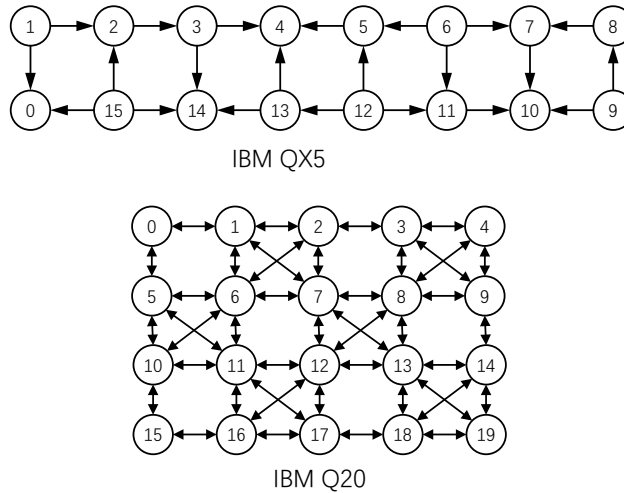


Figure 2: Two architecture graphs for IBM QX architecture.

classical bit, a qubit $|\psi\rangle$ can be in a linear combination of basis states [17], i.e.,

$$|\psi\rangle = \alpha |0\rangle + \beta |1\rangle \quad (1)$$

where $|\alpha|^2 + |\beta|^2 = 1$. Information processing or computation is realized by applying quantum gates on qubits. Typical gates which we are concerned with in this paper are Hadamard gate H, CNOT gate and SWAP gate, depicted in Fig. 1. H is a single-qubit gate which can evenly mix the basis states to produce a superposed one. CNOT and SWAP are both two-qubit gates, i.e., they operate on two qubits. A CNOT gate flips the target qubit (indicated graphically with \oplus) if and only if the control qubit (indicated graphically with a black dot \bullet) is in state $|1\rangle$, while a SWAP gate exchanges the states of the two qubits operated.

Quantum circuits are the most commonly used model to describe quantum algorithms, which consist of input qubits, quantum gates, measurements and classical registers [22]. However, as far as quantum circuit transformation is concerned, only input qubits and quantum gates are relevant. Thus in this paper, a quantum circuit is simply represented as a pair (Q, C) , where Q is the set of involved qubits and C a sequence of quantum gates. For a generic quantum circuit to be executed in a real quantum processing unit (QPU), two more steps have to be taken:

- *Compilation* process. As only limited quantum operations are available in a QPU, quantum gates in the circuit must be decomposed into elementary gates first [3, 9]. In this paper, we take single-qubit and CNOT gates as elementary gates as they are universal to implement any quantum circuit and supported by, say, IBM QX architectures.
- *Transformation* process. Qubits in a real QPU are typically laid out in a fixed topology and CNOT gates can only be applied on neighbouring qubits. Such a connectivity topology can be described by an *architecture graph* or *coupling graph* [6] which is a directed graph with each node representing a qubit in the QPU. A quantum circuit consisting of only single-qubit and CNOT gates is said to *respect* the QPU constraint if for every CNOT gate in the circuit, there is a directed edge in the architecture graph from the control qubit to the target qubit. The transformation process is then to convert a quantum circuit (say, those obtained from the above compilation process) into one that respects the QPU constraint so that it can be executed on the QPU.

In this paper, we only focus on the transformation process. The QPU topologies we are concerned with are IBM QX architectures QX5 and Q20 shown in Fig. 2, but our approach is applicable to any architecture graph, including for example Rigetti 16Q Aspen-4¹. Notice that edges in IBM Q20 are bidirectional (or, undirected)

¹<https://www.rigetti.com/qpu>

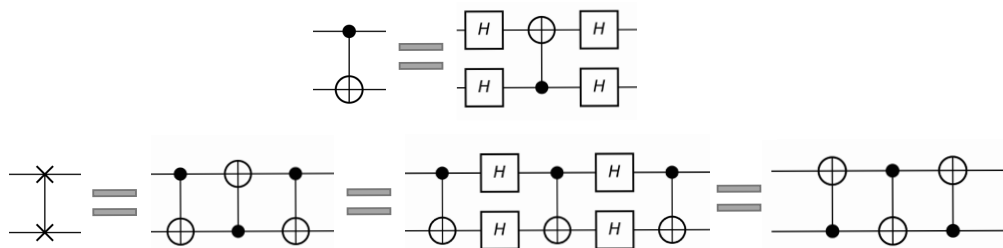


Figure 3: Some gate decomposition and transformation rules.

and thus either node of each edge can be the control qubit of a CNOT gate. Depicted in Fig. 3 are several gate transformation rules which are quite useful in gate decomposition and circuit transformation. The top equivalence shows that we can exchange the control and target qubits of a CNOT by adding two Hadamard gates before and after it, while the bottom ones show different ways of implementing a SWAP gate in QX structures.

To simplify the presentation, we distinguish between two kinds of quantum circuits in this paper. *Logical* circuits are ideal and high-level gate descriptions of quantum algorithms without considering any physical constraints imposed by QPUs. In contrast, *physical* quantum circuits are low-level gate-model implementation which respect the QPU concerned. The purpose of the circuit transformation process mentioned above is then to convert a logical circuit to a physical one. Accordingly, qubits appearing in logical circuits are called logical qubits while those appearing in physical circuits are called physical ones.

3 Quantum Circuit Transformation

The main objective of quantum circuit transformation is to transform an input logical circuit to a physical one so that the constraints imposed by the QPU are satisfied. To simplify the problem, we only consider the connectivity constraints for CNOT gates as specified by the architecture graph (see Section 2). This means that single-qubit gates have no effect in the circuit transformation process, and we assume without loss of generality that the input logical circuit consists only of CNOT gates. Furthermore, a CNOT gate is simply denoted as a pair $\langle q, q' \rangle$, where q is the control qubit and q' is the target qubit. We call the CNOT gate $\langle q', q \rangle$ the *inverse* of $\langle q, q' \rangle$.

Let $AG = (V, E)$ be the architecture graph of a QPU, where V is the set of physical qubits and E the set of directed edges along which CNOT gates can be performed. Given a logical circuit $LC = (Q, C^l)$ with $|Q| \leq |V|$, we need to construct a physical circuit $PC = (V, C^p)$ such that

- LC and PC are equivalent in functionality.
- C^p only contains CNOT gates and single qubit gates.
- For any CNOT gate $\langle q, q' \rangle$ in C^p , $(q, q') \in E$.

It is easy to find a physical circuit that satisfies the above conditions, but the real challenge is to find one with *minimal* size or depth, which is NP-hard in general [5]. In this paper, we modify the input logical circuit stepwise by inserting auxiliary gates like CNOT and H, as shown in Fig. 1, until the logical circuit is transformed into a physical circuit that can be executed on the QPU. To evaluate the effectiveness of quantum circuit transformation algorithms, we use the sizes of the output circuits, i.e., the total number of its elementary gates.

3.1 Dependency Graph

CNOT gates in a logic circuit $LC = (Q, C^l)$ are not independent. We say a CNOT gate $\langle q, q' \rangle$ *depends* on another $\langle p, p' \rangle$ if the latter must be executed before the former. This happens when $\langle p, p' \rangle$ is in front of $\langle q, q' \rangle$ in

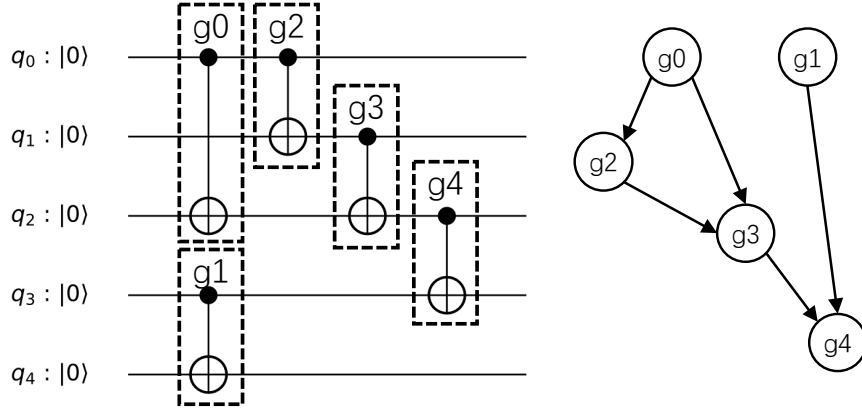


Figure 4: On the left is an example for logical quantum circuit with only CNOT gates and right DAG representing dependency order of the left circuit.

C^l and they share a common qubit (i.e., either $p \in \{q, q'\}$ or $p' \in \{q, q'\}$), or when $\langle q, q' \rangle$ depends on a CNOT gate which depends on $\langle p, p' \rangle$.

In general, we can construct a directed acyclic graph (DAG), called the *dependency graph* [10], to characterize the dependency between gates in a logical circuit LC [13]. Each node of the dependency graph represents a gate and each directed edge the dependency relationship from one gate to another. The front layer of LC , denoted $\mathcal{F}(LC)$ or $\mathcal{L}_0(LC)$, consists of all gates in LC which have no parents in the dependency graph. The second layer $\mathcal{L}_1(LC)$ is then the front layer of the circuit obtained from LC by deleting all gates in $\mathcal{F}(LC)$. Analogously, we can define the k -th layer $\mathcal{L}_k(LC)$ of LC for all $k \geq 0$. Consider the circuit shown in Fig. 4 as an example. Initially, gates g_0 and g_1 can be applied in parallel because there are no gates before them and they are independent from each other. Thus $\mathcal{F}(LC) = \{g_0, g_1\}$. Then, gate g_2 can be executed after g_0 , g_3 after g_2 and g_0 , and g_4 after g_3 and g_1 . Thus $\mathcal{L}_1(LC) = \{g_2\}$, $\mathcal{L}_2(LC) = \{g_3\}$, and $\mathcal{L}_3(LC) = \{g_4\}$.

3.2 Qubit Mapping

At each step of the circuit transformation, qubits in the logical circuit are mapped or allocated to physical qubits in the QPU [21]. Mathematically, a qubit mapping is a function τ from Q to V such that $\tau(q) = \tau(q')$ if and only if $q = q'$ for any $q, q' \in Q$ [6]. The mapping may change at consecutive steps of the transformation which is determined by the inserted auxiliary gates.

Given a logical circuit LC and a mapping τ , a CNOT gate $g = \langle q, q' \rangle$ in LC is said to be *satisfied* by τ , or τ *satisfies* g , if $(\tau(q), \tau(q'))$ is a directed edge in AG. Furthermore, g is *executable* by τ if it appears in the front layer of LC and is satisfied by τ . In this case, we remove it from LC and append a CNOT gate $\tau(g) := \langle \tau(q), \tau(q') \rangle$ to the end of the physical circuit. This process is called the *execution* of g .

4 The Proposed Algorithm

In this section, details of the proposed algorithm will be explained step by step. Let $AG = (V, E)$ be the architecture graph and $LC = (Q, C^l)$ the input logic circuit consisting only CNOT gates. The goal of the algorithm is to try to minimize the size, i.e., the total number of elementary gates, of the output physical circuit.

We first generate an initial mapping τ_{ini} by using simulated annealing (Algorithm 1), and then stepwise construct the output physical circuit by adding auxiliary CNOT or Hadamard gates while processing gates in the input logic circuit. The *state* of each step is described by a mapping τ' from logic qubits in Q to physical qubits in V , the currently constructed physical circuit PC' which obeys the constraints imposed by AG , and the logic circuit LC' with gates that have not been processed. A cost function which assigns decreasing weights

to gates in later layers is used to select the state of the next step. Note that the above procedure is standard for circuit transformation, and has been adopted in [25]. Our algorithm distinguishes itself from the previous ones in the ways of choosing the initial mapping (Sec 4.2), the definition of the cost function, and the strategy of updating step states (Sec 4.3).

4.1 CNOT Distance

In graph theory, the distance from a source node v to a destination node v' in a directed graph G , written $\text{dist}_G(v, v')$, is the minimal number of edges needed to traverse from v to v' . Suppose AG is the architecture graph of the QPU we consider. We define the *CNOT distance* from v to v' in AG, written $\text{dist}_{\text{cnot}}(v, v')$, as the minimal number of auxiliary CNOT and Hadamard gates required to execute the CNOT gate $\langle v, v' \rangle$ in the QPU. Here ‘execute’ is in the same sense as we have described in Section 3.2. To execute $\langle v, v' \rangle$, we need to bring the two qubits v and v' close to each other by swapping and then, when they are neighbours in AG, we further check if the direction is from v to v' or vice versa.

For bi-directed (or, undirected) architecture graph such as that of Q20, we need only to bring v close to v' or vice versa, and the CNOT distance is simply computed as $\text{dist}_{\text{cnot}}(v, v') = 3 \times (\text{dist}_{\text{AG}}(v, v') - 1)$. This is because only $\text{dist}_{\text{AG}}(v, v') - 1$ swaps are required and each SWAP requires only 3 CNOT gates to implement (see Fig. 3 (top)). For directed architecture graph such as that of QX5, the situation is a little complicated, where we also need to consider the direction of the CNOT gates. We first compute all shortest paths from v to v' (ignoring the directions). Suppose $d = \text{dist}_{\text{AG}}(v, v')$. If there is an undirected shortest path $\pi = \langle v_0 \equiv v, v_1, \dots, v_d \equiv v' \rangle$ in which (v_i, v_{i+1}) is a directed edge in QX5 for some i , then the CNOT distance is computed as $\text{dist}_{\text{cnot}}(v, v') = 7 \times (d - 1)$, because a SWAP gate is decomposed into 7 elementary gates (see Fig. 3 (bottom)). Otherwise, we have $\text{dist}_{\text{cnot}}(v, v') = 7 \times (d - 1) + 4$, as we need to add 2 Hadamard gates before and after to change the direction of the target CNOT [25].

Take QX5 as an example. Suppose the logic qubits q and q' are mapped to v_3 and v_1 , which correspond to nodes 3 and 1 in Fig. 2, respectively, and we want to implement the CNOT gate $\langle q, q' \rangle$, with q the control qubit and q' the target qubit. One solution is to add a SWAP gate between qubit v_1 and v_2 to bring q one step close to q' , and a CNOT gate between v_2 and v_3 together with 4 additional Hadamard gates (cf. Figure 3) to change the direction of the CNOT gate. Because a SWAP gate can be decomposed into 7 elementary gates complying with the directions in QX5, the CNOT distance from v_3 to v_1 in QX5 is 11.

For simplicity, in our algorithm we precompute the CNOT distance for all node pairs in AG by using, say, a breadth-first search algorithm.

4.2 Initial Mapping

The selection of a good initial mapping has a significant impact on the quality of the final physical circuit [19, 13, 25]. Intuitively, we would like to find an initial mapping that ‘fits’ most gates such that fewer SWAP gates are required in the circuit transformation process.

To this end, we define the *gate cost* of a CNOT gate $g = \langle q, q' \rangle$ under a mapping $\tau : Q \rightarrow V$ as

$$\text{cost}_{\text{gate}}(g, \tau) = \text{dist}_{\text{cnot}}(\tau(q), \tau(q')). \quad (2)$$

Our ideal initial mapping τ_{ini}^* is then given by

$$\tau_{\text{ini}}^* = \arg \min_{\tau} \left\{ \sum_{g \in C^*} \text{cost}_{\text{gate}}(g, \tau) \right\} \quad (3)$$

where C^* is a selected subset of the logical circuit LC . Here we use C^* instead of C^l to calculate the initial mapping. This is because taking into account all gates in C^l would bring further overhead and be unnecessary because gates in the tail of the circuit would have little impact on the initial mapping.

Simulated annealing (SA), inspired by the annealing process in metallurgy [11], is designed for approximating the global optimum of a given cost function. The algorithm tries to find the best state in the search space. In each trial for searching a better state, the algorithm generates a new state based on the previous one, calculates

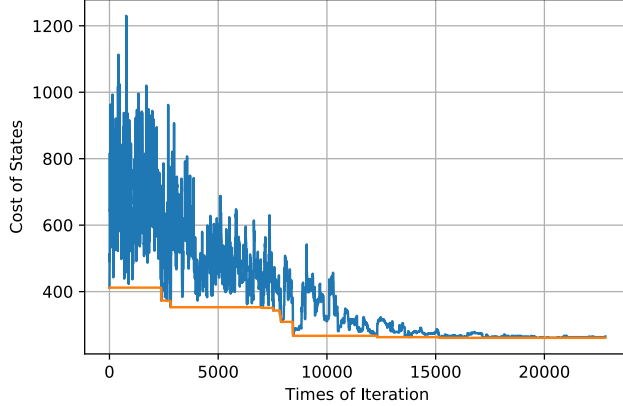


Figure 5: Convergence of the simulated annealing algorithm on circuit adr4-197 and IBM Q20, where the blue and orange lines represent the cost of accepted states and existing best states, respectively. We set empirically $T_{\max} = 100$, $T_{\min} = 1$, $\Delta = 0.98$, and $R = 100$.

its cost and compares it with the previous one and decides whether this new state should be accepted. To escape from local optima, the algorithm accepts the new generated state with a certain probability even if its cost is worse than the previous one. The acceptance probability is decided by the current temperature which declines during the search process until the minimum value is reached.

We propose an efficient simulated annealing based algorithm (Algorithm 1) to find a good approximation of τ_{ini}^* , where T_{\max} , T_{\min} , Δ and R are, respectively, the starting temperature, the minimum temperature, the decline coefficient for the temperature and the repeated times for one temperature. Fig. 5 shows convergence of the simulated annealing process on a real quantum circuit adr4-197. Note that the cost of states converges after sufficient iterations, showing that the temperature is low enough. The fluctuation of the cost of accepted states is caused by the above mentioned acceptance probability for worse states.

In the following two subsections, we describe in detail how to generate all possible child and grandchild states and how the cost of a child or grandchild state is calculated. We will illustrate the construction by using the quantum circuit shown in Fig. 6 and the test architecture graph AG_{test} in Fig. 7.

4.3 Heuristic search with look-ahead

We have shown in the previous section how to construct the initial mapping τ_{ini} for our circuit transformation algorithm, thus obtaining the state $s^0 := (\tau_{ini}, PC_0, LC_0)$ for the first step, where PC_0 and LC_0 are respectively the physical and logic circuits after executing all gates in LC which are executable in τ_{ini} . Suppose we are in state $s^i := (\tau_i, PC_i, LC_i)$ at the i -th step for $i \geq 0$. This section is devoted to the strategy of choosing s^{i+1} for the $i+1$ -th step. Obviously, depending on the different ways of adding auxiliary CNOT and H gates, there are multiple child states of s^i to choose from. One natural way is to select the one with the minimal cost. This surely gives a fine method for extending s^i , but (as shown in Fig. 10) the sizes of the output physical circuits are not always desirable. In this paper, we propose a novel way to select the next state: we look one level ahead to calculate the costs of all *grandchild* states of s^i , and choose the child of s^i which has a child (thus a grandchild of s^i) with the minimum cost among all grandchildren of s^i .

To this end, we have to specify for a given state $s^i := (\tau_i, PC_i, LC_i)$, (1) how to extend s^i to get all its children and grandchildren, and (2) how to define the costs of its grandchildren. We are going to elaborate these two points one by one in the following.

Extend s^i . There are two natural ways to extend s^i .

- Way 1: Apply on τ_i a swap operation represented as an edge in AG one of whose end nodes is the image under τ_i of some qubit appearing in a gate in the front layer of LC_i , and obtain a new mapping τ_i^l .

Algorithm 1: Simulated annealing for computing the initial mapping

input : A set C^* for considered gates in a logical quantum circuit.
output: An approximation of the optimal initial mapping given in Eq.(3).
begin
 Initialize parameters T_{\max} , T_{\min} , Δ , R , and an arbitrary mapping τ ;
 $T \leftarrow T_{\max}$, $bcost \leftarrow \infty$, $cost \leftarrow \infty$;
 while $T \geq T_{\min}$ **do**
 $i \leftarrow 1$;
 while $i \leq R$ **do**
 $i \leftarrow i + 1$;
 Change mapping τ randomly to generate a new mapping τ_{new} ;
 $ncost = \sum_{g \in C^*} \text{cost}_{gate}(g, \tau_{new})$;
 if $ncost < bcost$ **then**
 $bcost \leftarrow ncost$;
 $\tau_{ini} \leftarrow \tau_{new}$;
 end
 if $ncost < cost$ **then**
 $cost \leftarrow ncost$;
 $\tau \leftarrow \tau_{new}$;
 else
 $cost \leftarrow ncost$ and $\tau \leftarrow \tau_{new}$ with prob. $\exp(\frac{cost-ncost}{T})$;
 end
 end
 $T \leftarrow \Delta \times T$;
 end
 return τ_{ini}
end

Accordingly, we extend PC_i with the CNOT + H implementation of the SWAP gate corresponding to this swap operation. Then we execute recursively all gates in LC_i (not only those in the front layer, but also those executable when their precedents have already been executed by τ'_i) which are executable in τ'_i . The resultant state is then a child of s^i .

- Way 2 only applies when AG is directed and there is a CNOT gate $\langle q, q' \rangle$ in the front layer of LC_i which is inversely executable, i.e. its inverse gate $\langle q', q \rangle$ is executable, in τ_i . In this case, we add 4 Hadamard gates to change the direction of $\langle q, q' \rangle$ (cf. Figure 3 (top)), extend PC_i with all these 5 gates, and delete $\langle q, q' \rangle$ from LC_i . Again, we execute recursively all gates in LC_i which are executable in τ_i to get a child of s^i .

Finally, for each child of s^i , we extend one level further to get its grandchildren. We denote by $\{s^i_j : j \in J\}$ and $\{s^i_{j,k} : j \in J, k \in K\}$ the set of children and grandchildren of s^i , respectively.

Example 1. We consider the quantum circuit shown in Fig. 6 and the test architecture graph AG_{test} in Fig. 7. Applying Alg. 1 we get the initial mapping $\tau_{ini} : Q \rightarrow V$ which maps q_i to v_i for each $0 \leq i \leq 4$. For convenience, we write such a mapping as a list of length 5. For example, $\tau_{ini} = [0, 1, 2, 3, 4]$. Note that the front layer contains two gates, viz., $\langle q_2, q_1 \rangle$ and $\langle q_3, q_4 \rangle$. As the latter is directly executable by τ_{ini} , the initial state $s = (\tau_{ini}, PC_0 := \{\langle q_3, q_4 \rangle\}, LC_0 := LC \setminus \{\langle q_3, q_4 \rangle\})$, where LC is the circuit shown in Fig. 6.

We next show how to construct the child states of s . Note that there is only one gate, viz. $\langle q_2, q_1 \rangle$, in the first layer of LC_0 , and τ_{ini} maps q_1 and q_2 to, respectively, v_1 and v_2 . Only 4 edges, $(1, 0)$, $(1, 2)$, $(2, 3)$ and $(5, 2)$, in AG_{test} (see Fig. 7) are relevant. For each of them, we obtain a corresponding swap operation and a corresponding child state. Since AG_{test} is directed and τ_{ini} can execute $\langle q_1, q_2 \rangle$, another child state can be obtained by using Way 2. Therefore, s has in total 5 child states and Table 1 gives the mappings and physical circuits of these child states as well as the corresponding operations. Similarly, we also construct the grandchild

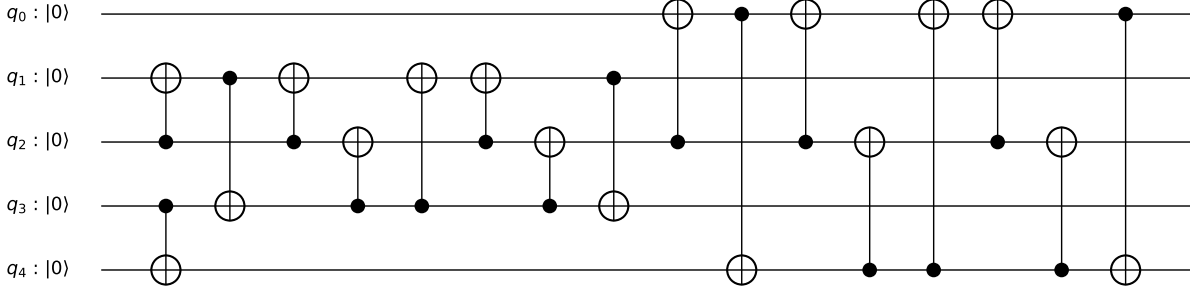


Figure 6: The quantum circuit alu-v0_27 with all single qubit gates removed.

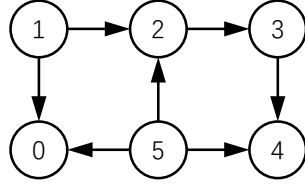


Figure 7: A test architecture graph AG_{test} .

states of s , also shown in Table 1. Here in the ‘Operation’ column, we use an edge in AG_{test} to denote the corresponding swap operation on mappings, and a CNOT gate to denote the operation of changing its direction.

Evaluate the grandchildren of s^i . The cost of a grandchild $s_{j,k}^i$ of s^i consists of two parts: the first part, $\text{cost}_g(s_{j,k}^i)$, is the number of auxiliary CNOT and Hadamard gates added during the evolution from s^i to $s_{j,k}^i$, and the second part, $\text{cost}_h(s_{j,k}^i)$, is an estimated cost for completing the remaining gates in the logic circuit of $s_{j,k}^i$.

The first part depends on the different ways of extending s^i and s_j^i to obtain $s_{j,k}^i$. If AG is undirected, then only Way 1 is available for the extensions and 3 CNOT gates suffice to implement the required swap operation on the mapping. Thus $\text{cost}_g(s_{j,k}^i) = 6$. Otherwise, 7 gates (3 CNOTs and 4 Hadamard shown in Fig. 3) for Way 1 and 4 Hadamard for Way 2 are needed. Thus $\text{cost}_g(s_{j,k}^i)$ can be 14, 11, or 8. Consider the state s in Example 1. From Table 1 we can see that each grandchild state of s has cost_g 14 or 11.

For the second part of the cost, we employ a look-ahead mechanism first demonstrated in [13]. Given a generic state $s = (\tau_s, PC_s, LC_s)$, we partition the gates in LC_s into different layers according to its dependency graph. Denote by L_k , $k \geq 0$, these layers such that L_0 is the front layer. Then the heuristically estimated cost of s is defined as

$$\text{cost}_h(s) = \sum_{k=0}^{\ell} w_k \left(\sum_{g \in L_k} \text{cost}_{\text{gate}}(g, \tau_s) \right) + w_s \times (d - 1) \times N_{\text{swap}} \times N_s, \quad (4)$$

where d is the diameter of the architecture graph, N_{swap} the number of elementary gates needed to compose a SWAP gate, and N_s is the number of gates in LC_s . The parameters $\ell > 0$, w_k ($0 \leq k \leq \ell$) and w_s are taken empirically but normally we assume $1 = w_0 \geq w_1 \geq \dots \geq w_\ell \geq w_s \geq 0$. This reflects the intuition that the closer a gate is from the front layer of the circuit, the more it contributes to the total cost of executing the whole circuit, as subsequent dependent gates will not be executable unless it has been processed. Table 1 gives the heuristic costs for all child and grandchild states of s in Example 1, where we take $\ell = 3$, $w_1 = 1$, $w_2 = 0.8$, $w_3 = 0.6$, $w_s = 0.4$. Note that the diameter of QX5 is 8 and each SWAP gate is composed by 7 elementary gates in QX5. Thus $d = 8$ and $N_{\text{swap}} = 7$.

Finally, the total cost of a grandchild $s_{j,k}^i$ of s^i is computed as

$$\text{cost}(s_{j,k}^i) = \text{cost}_g(s_{j,k}^i) + \text{cost}_h(s_{j,k}^i). \quad (5)$$

Child State	Mapping	Newly added gates in PC_s	Operation	cost_g	cost_h
s_0	[1,0,2,3,4]	$\{0 \leftrightarrow 1\}$	(1,0)	7	208.2
s_1	[1,0,2,3,4]	$\{1 \leftrightarrow 2, \langle 1, 2 \rangle, \langle 2, 3 \rangle, \langle 1, 2 \rangle\}$	(1,2)	7	167.2
s_2	[0,1,3,2,4]	$\{2 \leftrightarrow 3\}$	(2,3)	7	199.0
s_3	[0,1,5,3,4]	$\{5 \leftrightarrow 2\}$	(5,2)	7	203.0
s_4	[0,1,2,3,4]	$\langle 1, 2 \rangle$	$\langle q_2, q_1 \rangle$	4	188.8
$s_{0,0}$	[0,1,2,3,4]	$\{0 \leftrightarrow 1\}$	(0,1)	14	195.8
$s_{0,1}$	[1,5,2,3,4]	$\{0 \leftrightarrow 5\}$	(0,5)	14	195.8
$s_{0,2}$	[2,0,1,3,4]	$\{1 \leftrightarrow 2, \langle 1, 0 \rangle\}$	(1,2)	14	199.2
$s_{0,3}$	[1,0,3,2,4]	$\{2 \leftrightarrow 3\}$	(2,3)	14	211.4
$s_{0,4}$	[1,0,5,3,4]	$\{2 \leftrightarrow 5, \langle 5, 0 \rangle\}$	(2,5)	14	196.0
$s_{1,0}$	[1,2,0,3,4]	$\{0 \leftrightarrow 1\}$	(0,1)	14	177.6
$s_{1,1}$	[0,1,2,3,4]	$\{1 \leftrightarrow 2\}$	(1,2)	14	166.2
$s_{1,2}$	[0,3,1,2,4]	$\{2 \leftrightarrow 3\}$	(2,3)	14	157.6
$s_{1,3}$	[0,2,1,4,3]	$\{3 \leftrightarrow 4\}$	(3,4)	14	175.0
$s_{2,0}$	[1,0,3,2,4]	$\{0 \leftrightarrow 1\}$	(0,1)	14	211.4
$s_{2,1}$	[0,2,3,1,4]	$\{1 \leftrightarrow 2\}$	(1,2)	14	194.6
$s_{2,2}$	[0,1,2,3,4]	$\{2 \leftrightarrow 3\}$	(2,3)	14	195.8
$s_{2,3}$	[0,1,4,2,3]	$\{3 \leftrightarrow 4\}$	(3,4)	14	208.6
$s_{3,0}$	[1,0,5,3,4]	$\{0 \leftrightarrow 1, \langle 5, 0 \rangle\}$	(0,1)	14	196.0
$s_{3,1}$	[5,1,0,3,4]	$\{0 \leftrightarrow 5\}$	(0,5)	14	201.8
$s_{3,2}$	[0,2,5,3,4]	$\{1 \leftrightarrow 2, \langle 5, 2 \rangle, \langle 2, 3 \rangle, \langle 5, 2 \rangle\}$	(1,2)	14	160.8
$s_{3,3}$	[0,1,2,3,4]	$\{2 \leftrightarrow 5\}$	(2,5)	14	195.8
$s_{3,4}$	[0,1,4,3,5]	$\{4 \leftrightarrow 5\}$	(4,5)	14	211.4
$s_{4,0}$	[1,0,2,3,4]	$\{0 \leftrightarrow 1\}$	(0,1)	11	200.6
$s_{4,1}$	[0,2,1,3,4]	$\{1 \leftrightarrow 2, \langle 2, 3 \rangle, \langle 1, 2 \rangle\}$	(1,2)	11	167.2
$s_{4,2}$	[0,1,3,2,4]	$\{2 \leftrightarrow 3, \langle 1, 2 \rangle\}$	(2,3)	11	177.6
$s_{4,3}$	[0,1,2,4,3]	$\{3 \leftrightarrow 4\}$	(3,4)	11	200.0

Table 1: The child and grandchild states of $s = (\tau_{ini}, PC_0 := \{\langle q_3, q_4 \rangle\}, LC_0 := LC \setminus \{\langle q_3, q_4 \rangle\})$ in Example 1, where $i \leftrightarrow j$ denotes the swap operation of i and j and $\langle i, j \rangle$ denotes the operation that changes the direction of the CNOT gate $\langle i, j \rangle$.

Suppose s_{j^*, k^*}^i is a grandchild state with the minimum cost. Then $s_{j^*}^i$ is selected as the state for the $i + 1$ -th step; that is, we let $s^{i+1} = s_{j^*}^i$. For the state s in Example 1, we can see from Table 1 that $s_{1,2}$ is the grandchild state with minimum cost. Thus we select its parent s_1 as our next state. Note that s_1 happens to be the child state which also has the minimum cost among all child states of s . In general, this coincidence does not hold. The whole algorithm for circuit transformation is shown in Algorithm 2.

4.4 Fallback via remote CNOT

During the search process, there is a small possibility that our algorithm does not halt. This happens when a child state with better cost may be good for gates in look-ahead layers but increases the distances of gates in the front layer. To address this problem, a fallback mechanism is introduced to ensure that the program terminates in reasonable time.

A direct way for fallback is to select a gate $\langle q, q' \rangle$ in the front layer and then choose a SWAP operation that will reduce the shortest path between the two corresponding nodes v, v' with $\tau_s(q) = v$ and $\tau_s(q') = v'$ in the architecture graph [6], where s denotes the current state. However, this method may change the mapping that the algorithm may want to keep as it is preferred by look-ahead layers. To protect the preferred mapping, remote CNOT operations [18], which are depicted in Fig. 8, are introduced in the fallback. After imposing remote CNOT gates, the circuit has the same functionality while preserving the current mapping. The fallback is activated when no gates are removed from LC_s after a certain prefixed number of rounds.

Algorithm 2: Circuit transformation with look-ahead

input : A logic circuit $LC = (Q, C^l)$, an initial mapping τ constructed by Algorithm 1 and an architecture graph $AG = (V, E)$ with $|Q| \leq |V|$.

output: A physical circuit (V, C^p) which satisfies AG and is equivalent to LC .

begin

$(PC, LC) \leftarrow \text{Execute}(\tau, PC, LC)$;

while $LC \neq \emptyset$ **do**

$L \leftarrow \mathcal{F}(LC)$, the first layer of LC ;

$Cld \leftarrow \emptyset$;

for $e \in E$ which touches some gate in L under τ **do**

$\tau' \leftarrow \text{swap}_e \circ \tau$;

$PC' \leftarrow PC'$ by adding (the $CNOT + H$ implementation of) a SWAP gate corresponding to swap_e ;

$(PC', LC') \leftarrow \text{Execute}(\tau', PC', LC)$;

$gcost \leftarrow 3$ if $e^{-1} \in E$ and 7 otherwise;

$Cld \leftarrow Cld \cup \{(\tau', PC', LC', gcost)\}$;

end

for $g \in L$ which is inversely executable by τ **do**

$PC' \leftarrow PC'$ by adding $\tau(g)$ complemented by four H gates before and after it;

$LC' \leftarrow LC'$ by deleting g ;

$(PC', LC') \leftarrow \text{Execute}(\tau, PC', LC')$;

$Cld \leftarrow Cld \cup \{(\tau, PC', LC', 4)\}$;

end

$mCost \leftarrow \infty$;

for $(\tau', PC', LC', gcost) \in Cld$ **do**

$cost \leftarrow \text{minChildHcost}(\tau', LC')$;

if $cost + gcost < mCost$ **then**

$mCost \leftarrow cost + gcost$;

$(\tau, PC, LC) \leftarrow (\tau', PC', LC')$;

end

end

end

return PC

end

Procedure $\text{Execute}(\tau, PC, LC)$

input : A mapping $\tau : Q \rightarrow V$, a physical circuit PC , and a logic circuit LC .

output: A pair (PC', LC') obtained by executing as many as possible gates which satisfy τ .

begin

$PC' \leftarrow PC$; $LC' \leftarrow LC$;

do

$EL \leftarrow \{g \in \mathcal{F}(LC') : g \text{ is executable by } \tau\}$;

for $g \in EL$ **do**

$PC' \leftarrow PC'$ by adding $\tau(g)$;

$LC' \leftarrow LC'$ by deleting g ;

end

while $EL \neq \emptyset$;

return (PC', LC')

end

Procedure minChildHcost(τ, LC)

input : A mapping $\tau : Q \rightarrow V$ and a logic circuit LC .

output: The minimal cost of all children of τ .

begin

$L \leftarrow \mathcal{F}(LC)$;

$mCost \leftarrow \infty$;

for $e \in E$ which touches some gate in L under τ **do**

$\tau' \leftarrow \text{swap}_e \circ \tau$;

$(PC', LC') \leftarrow \text{Execute}(\tau', \emptyset, LC)$;

$gcost \leftarrow 3$ if $e^{-1} \in E$ and 7 otherwise;

$hcost \leftarrow hcost(\tau', LC')$ according to Eq.(4);

if $hcost + gcost < mCost$ **then**

$mCost \leftarrow hcost + gcost$;

end

end

for $g \in L$ which is inversely executable by τ **do**

$LC' \leftarrow LC$ by deleting g ;

$(PC', LC') \leftarrow \text{Execute}(\tau, \emptyset, LC)$;

$hcost \leftarrow hcost(\tau, LC')$ according to Eq.(4);

if $hcost + 4 < mCost$ **then**

$mCost \leftarrow hcost + 4$;

end

end

return $mCost$;

end

4.5 Complexity of the Search Process

In each layer, there are at most $|Q|/2$ gates, where Q is the set of qubits in the input logic circuit. Thus, the time complexity of computing the cost (cf. Eq.(5)) of any state is $O(\ell \cdot |Q|)$, where ℓ is the prefixed small number of layers we select for Eq.(4). For our evaluation (see Section 5), we take $\ell = 3$ for all circuits.

By construction, each state s has at most $|E| + |Q|/2$ child states, where E is the set of edges in the architecture graph, or, equivalently, the number of possible SWAP operations that can be added to the circuit and $|Q|/2$ is the number of CNOT gates in the front layer of the current logic circuit that can be applied by adding four extra Hadamard gates to change the direction.

Suppose the input circuit contains m CNOT gates. If we activate the fallback when no gates are removed from LC_s after K rounds, then the search procedure has at most $K \times m$ states. This is because each activation of the fallback will execute a selected gate due to the use of remote CNOT. Therefore, the overall time complexity of the search is $O(\ell \cdot |Q| \cdot (|E| + |Q|/2)^2 \cdot m \cdot K)$. Because $|Q| \leq |V|$ and $|E| \leq |V| \cdot (|V| - 1)/2$, it is bounded by $O(|V|^4 \cdot |Q| \cdot \ell \cdot m \cdot K)$.

For the space complexity, in each state s , we maintain a depth-2 search tree rooted at s . Thus the space complexity of the algorithm is bounded by $O((|E| + |Q|/2)^2)$, i.e., $O(|V|^4)$.

4.6 Optimization

In Algorithm 2, the search space grows exponentially if the depth of look-ahead is increased. Therefore, a pruning mechanism is introduced to reduce the size of the search space while preserving the quality of the output physical circuit. More specifically, a child state s_j^i of s^i will be removed if both $\text{cost}'_h(s_j^i) > \text{cost}'_h(s^i)$ and $\text{cost}_h(s_j^i) - \text{cost}'_h(s_j^i) > \text{cost}_h(s^i) - \text{cost}'_h(s^i)$, where $\text{cost}'_h(s) = w \times (d-1) \times N_{\text{swap}} \times N_s s$ as defined in Eq.(4). In Example. 1, states $s_{1,0}$ will be pruned. This is because $\text{cost}'_h(s) = 145.6$, $\text{cost}_h(s) = 167.2$, $\text{cost}'_h(s_0) = 145.6$, $\text{cost}_h(s_0) = 177.6$ and $\text{cost}_h(s_0) > \text{cost}_h(s)$, $\text{cost}_h(s_0) - \text{cost}'_h(s_0) > \text{cost}_h(s) - \text{cost}'_h(s)$.

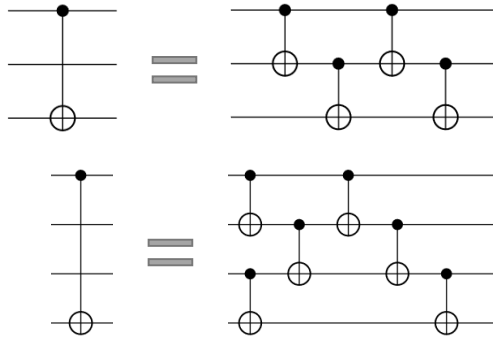


Figure 8: Schematic for remote CNOT operations with 2 and 3 hops. Generalized form can be found in [16].

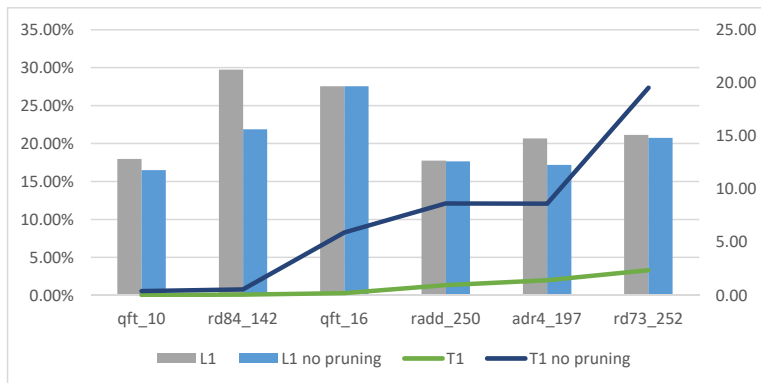


Figure 9: Effectiveness of the pruning mechanism obtained by running exemplary circuits on IBM Q20, where the gray and blue bars are ratios of the number of added gates to that of original gates for the proposed algorithm with and without pruning while lines correspond to the time consumption (seconds) for the search process.

From Fig. 9 we can see that the pruning mechanism has limited influence on the sizes of the output circuits while the time consumption is reduced by a large amount.

5 Programming and Benchmarks

To evaluate our approach, we compare it with previous algorithms proposed for the same purpose in the literature [25, 13, 7]. We use Python as our programming language and IBM Qiskit [1] as auxiliary environment. The code can be found in GitHub². All experiments are conducted in a laptop with i7-8750H CPU and 16GB memory. The results are reported in Tables 2, 3 and 4, in which the ‘Comparison’ column shows the improvement of our algorithm over previous ones in terms of the numbers of auxiliary gates added. Specifically, let n_{comp} and n_{ours} be the numbers of gates added by the compared algorithm and by ours, respectively. Then the improvement ratio is defined as $(n_{comp} - n_{ours})/n_{comp}$.

Table 2 demonstrates the superiority of the initial mapping output by our simulated annealing algorithm (Alg. 1) compared to the naive initial mapping which maps q_i to v_i for all i in Q20. The improvement is consistent and often above 30%.

For the heuristic search, we compare our algorithm to the ones introduced in [25] and [13], which are, respectively, the state-of-the-art algorithms for IBM QX5 and Q20. We set the number of look-ahead layers as $\ell = 3$, and the weight parameters $w_1 = 1$, $w_2 = 0.8$, $w_3 = 0.6$, $w_4 = 0.4 \times (D_{AG} - 1) \times N_{swap}$ in Eq.(4), where

²<https://github.com/BensonZhou1991/circuittransform/>

Circuit Name	Original Gates	Naive Mapping	Simulated Annealing	Improvement
4mod5-v1_22	21	30	21	100.00%
mod5mils_65	35	56	35	100.00%
alu-v0_27	36	51	42	60.00%
decod24-v2_43	52	85	52	100.00%
4gt13_92	66	120	66	100.00%
ising_model_10	480	528	480	100.00%
ising_model_13	633	687	633	100.00%
ising_model_16	786	882	786	100.00%
qft_10	200	290	236	60.00%
qft_16	512	740	647	40.79%
rd84_142	343	490	445	30.61%
adr4_197	3439	4483	4150	31.90%
radd_250	3213	4182	3942	24.77%
z4_268	3073	3925	3619	35.92%
sym6_145	3888	4734	4632	12.06%
misex1_241	4813	5830	5734	9.44%
rd73_252	5321	7124	6446	37.60%
cycle10_2_110	6050	7433	7088	24.95%
square_root_7	7630	9250	8983	16.48%
sqn_258	10223	13328	12176	37.10%
rd84_253	13658	17798	16856	22.75%
co14_215	17936	22814	22292	10.70%
sym9_193	34881	44544	41004	36.63%
9symml_195	34881	44544	40917	37.53%

Table 2: The performance improvement brought by simulated annealing on IBM Q20. Here we compare with the naive mapping $\tau_{nv} : Q \rightarrow V$ which maps q_i to v_i for all i in Q20.

D_{AG} is the diameter of the architecture graph and N_{swap} the number of elementary gates needed to compose a SWAP gate. The threshold number K for activating fallback is set to be $0.5 \times D_{AG}$.

The algorithm proposed in [25] utilizes A^* to find the best solution of each layer. It has exponential time complexity and only considers one layer for look-ahead when designing the heuristic cost function. Like ours, their A^* -based algorithm works for both directed and undirected architecture graphs. As confirmed in [13], it is comparable with the algorithm in [13] when Q20 is used as the QPU. So we only make the comparison on QX5. From the experimental results reported in Table 3, we can see that our algorithm has a conspicuous improvement over the algorithm in [25]. Moreover, it is very efficient: for input circuits with up to 10,000 elementary gates, our algorithm finds the solution within one minute.

The algorithm proposed in [13] uses reverse traversal technique to search for a good initial mapping and has polynomial complexity. Although it considers multiple levels in its heuristic function, this algorithm does not consider the weights for gates in different layers in the heuristic function. Unlike our algorithm, the algorithm in [13] can only be applied to undirected architecture graphs. Therefore, we only compared it with ours on Q20. From the experimental results reported in Table 4, we see that, for small circuits, both algorithms find the optimal output circuits; but for circuits with large size, our algorithm again has a conspicuous improvement. As for QX5, our algorithm is able to find within two minutes the solution to input circuits with up to 30,000 elementary gates.

We also compared our algorithm with the algorithm proposed in [7], which also works for both directed and undirected architecture graph and its performance is comparable with the one in [25]. In Appendix, from the experimental results reported in Table 5 and 6, we can see that our algorithm also has a better performance.

It is worth mentioning that, if the depth for look-ahead in the selection process is increased, the quality of the output circuits could be further improved. However, the time consumption will be increased dramatically. See Fig. 10 for the experiment on a few examples, which indicates that 1-depth look-ahead reaches the best

Circuit Name	Original Gates	Algorithm in [25]	Proposed Algorithm	Running Time(s)	Improvement
mini_alu_305	173	734	545	0.27	33.69%
qft_10	200	637	473	0.30	37.53%
sys6-v0_111	215	940	701	0.32	32.97%
rd73_140	230	934	734	0.42	28.41%
sym6_316	270	1145	925	0.43	25.14%
rd53_311	275	1092	985	0.44	13.10%
sym9_146	328	1317	1105	0.53	21.44%
rd84_142	343	1381	1125	0.59	24.66%
ising_model_10	480	680	622	0.65	29.00%
cnt3-5_180	485	1703	1553	0.83	12.32%
qft_16	512	1776	1402	0.91	29.59%
ising_model_13	633	913	832	1.36	28.93%
ising_model_16	786	1106	1049	1.64	17.81%
wim_266	986	3867	3057	1.86	28.12%
cm152a_212	1221	4528	3834	1.95	20.99%
cm42a_207	1776	6209	5612	3.39	13.47%
pm1_249	1776	6209	5576	3.42	14.28%
dc1_220	1914	7009	5957	3.44	20.65%
squar5_261	1993	7348	6641	4.60	13.20%
sqrt8_260	3009	11340	10181	8.05	13.91%
z4_268	3073	11193	9995	8.40	14.75%
adr4_197	3439	12712	11523	8.70	12.82%
sym6_145	3888	13426	11794	10.95	17.11%
misex1_241	4813	17433	15714	14.74	13.62%
square_root_7	7630	Time Out	25972	44.05	#
ham15_107	8763	31743	28829	44.66	12.68%
dc2_222	9462	35903	32417	58.38	13.18%
sqn_258	10223	36957	33074	58.91	14.52%
inc_237	10619	39151	35515	59.28	12.74%
co14_215	17936	69830	61360	320.81	16.32%
life_238	22445	82117	75272	265.09	11.47%
max46_240	27126	96852	88955	395.91	11.33%
9symml_195	34881	130153	117191	667.18	13.61%
dist_223	38046	141729	130091	829.44	11.22%
sao2_257	38577	146996	132110	1059.06	13.73%
plus63mod4096_163	128744	Time Out	445208	9669.79	#
Summarizing	250896	927063	836749	#	13.36%

Table 3: Comparison of our algorithm with the A^* -based algorithm in [25] on IBM QX5.

Circuit Name	Original Gates	Algorithm in [13]	Proposed Algorithm	Running Time(s)	Improvement
4mod5-v1_22	21	21	21	0.00	0.00%
mod5mils_65	35	35	35	0.00	0.00%
alu-v0_27	36	39	42	0.00	-75.00%
decod24-v2_43	52	52	52	0.00	0.00%
4gt13_92	66	66	66	0.00	0.00%
ising_model_10	480	480	480	0.00	0.00%
ising_model_13	633	633	633	0.01	0.00%
ising_model_16	786	786	786	0.01	0.00%
qft_10	200	254	236	0.16	32.73%
qft_16	512	698	647	0.38	27.27%
rd84_142	343	448	445	1.50	2.83%
adr4_197	3439	5053	4150	2.08	55.91%
radd_250	3213	4488	3942	2.13	42.79%
z4_268	3073	4438	3619	2.65	59.96%
sym6_145	3888	5160	4632	2.82	41.48%
misex1_241	4813	6334	5734	3.44	39.42%
rd73_252	5321	7454	6446	5.21	47.24%
cycle10_2_110	6050	8672	7088	5.46	60.39%
square_root_7	7630	10228	8983	12.24	47.90%
sqn_258	10223	14567	12176	13.91	55.03%
rd84_253	13658	19805	16856	34.75	47.97%
co14_215	17936	26918	22292	88.90	51.50%
sym9_193	34881	51534	41004	126.68	63.23%
9symml_195	34881	52149	40917	137.47	65.04%
Summarizing	152170	220312	181282	#	57.28%

Table 4: Comparison of our algorithm with the algorithm in [13] on IBM Q20.

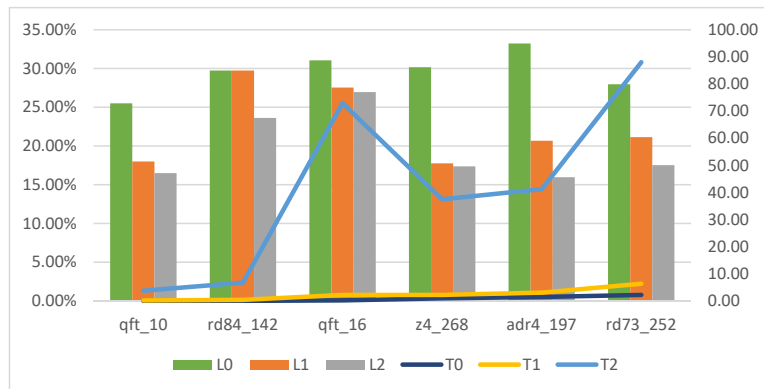


Figure 10: Experiments on IBM Q20 for different look-ahead depths. The vertical axis on the left is the ratio of the number of added gates to that of the original gates, and the right axis shows the consumed time. The bar and line represent respectively the number of gates and the consumed time for different circuits and different look-ahead depths.

trade off of time and performance. Although the time overhead for increasing the depth is vast, it may still be acceptable in some application scenarios and this can easily be done by adjusting the relevant parameters of our algorithm. Besides, the weight parameters in the heuristic function are also adjustable when different architecture graphs and circuits are considered.

6 Conclusion

In this paper, we propose an algorithm to solve the quantum circuit transformation problem by using simulated annealing and heuristic search. A double look-ahead mechanism is novelly adopted in the algorithm. We look ahead at subsequent layers when defining a flexible heuristic cost function which also supports weight parameters to reflect the variable influence of gates in different layers. Moreover, we look ahead at grandchild states with minimal cost in selecting the best state for the next step of the circuit transformation. Detailed evaluation on extensive realistic circuits shows that our algorithm has consistent and significant improvement when compared with the two state-of-the-art algorithms proposed in the literature for IBM QX5 and Q20.

For future studies, we propose the following problems to solve. First, our program still runs slowly for circuits with large sizes. Thus it is necessary to optimize the code to reduce the running time. Second, the quality of the initial mappings obtained from the simulated annealing algorithm (Alg. 1) is not stable, which is not acceptable for commercial use. Third, we only consider connectivity in the architecture graphs; other constraints like cross talk, gate error and qubits decoherence should be included to make the algorithm more practical. Fourth, only using the sizes of circuits as the criterion for evaluation is not enough. Criteria like circuit error and running time should also be considered in future work.

A More experimental results

Circuit Name	Original Gates	Algorithm in [7]	Proposed Algorithm	Running Time(s)	Improvement
graycode6_47	5	13	13	0.00	0.00%
xor5_254	7	30	14	0.00	69.57%
ex1_226	7	30	21	0.00	39.13%
4gt11_84	18	55	47	0.01	21.62%
ex-1_166	19	68	48	0.01	40.82%
ham3_102	20	76	52	0.01	42.86%
4mod5-v0_20	20	61	49	0.01	29.27%
4mod5-v1_22	21	62	53	0.01	21.95%
mod5d1_63	22	78	58	0.02	35.71%
4gt11_83	23	82	63	0.02	32.20%
4gt11_82	27	109	78	0.03	37.80%
rd32-v0_66	34	108	91	0.02	22.97%
mod5mils_65	35	132	88	0.02	45.36%
4mod5-v0_19	35	128	95	0.02	35.48%
rd32-v1_68	36	110	93	0.02	22.97%
alu-v0_27	36	118	97	0.02	25.61%
3_17_13	36	102	93	0.02	13.64%
4mod5-v1_24	36	113	96	0.02	22.08%
alu-v1_29	37	119	98	0.02	25.61%
alu-v1_28	37	131	105	0.02	27.66%
alu-v3_35	37	119	106	0.02	15.85%
alu-v2_33	37	119	91	0.02	34.15%
alu-v4_37	37	119	98	0.02	25.61%
miller_11	50	169	139	0.03	25.21%
decod24-v0_38	51	154	126	0.03	27.18%
alu-v3_34	52	181	160	0.03	16.28%
decod24-v2_43	52	155	141	0.02	13.59%
mod5d2_64	53	162	163	0.03	-0.92%
4gt13_92	66	218	187	0.04	20.39%
4gt13-v1_93	68	212	186	0.05	18.06%
one-two-three-v2_100	69	217	199	0.04	12.16%
4mod5-v1_23	69	234	214	0.05	12.12%
4mod5-v0_18	69	215	212	0.05	2.05%
one-two-three-v3_101	70	244	199	0.06	25.86%
4mod5-bdd_287	70	219	200	0.04	12.75%
decod24-bdd_294	73	216	206	0.04	6.99%
4gt5_75	83	263	226	0.05	20.56%
alu-v0_26	84	281	248	0.06	16.75%
rd32_270	84	264	245	0.05	10.56%
alu-bdd_288	84	245	247	0.07	-1.24%
decod24-v1_41	85	281	245	0.05	18.37%
4gt5_76	91	302	271	0.08	14.69%
4gt13_91	103	348	293	0.08	22.45%
4gt13_90	107	371	319	0.09	19.70%
alu-v4_36	115	375	326	0.08	18.85%
4gt5_77	131	409	363	0.10	16.55%
one-two-three-v1_99	132	447	392	0.09	17.46%
rd53_138	132	412	381	0.22	11.07%
one-two-three-v0_98	146	445	428	0.12	5.69%

Circuit Name	Original Gates	Algorithm in [7]	Proposed Algorithm	Running Time(s)	Improvement
4gt10-v1_81	148	506	422	0.10	23.46%
decod24-v3_45	150	496	407	0.11	25.72%
aj-e11_165	151	472	409	0.11	19.63%
4mod7-v0_94	162	540	456	0.14	22.22%
alu-v2_32	163	517	472	0.13	12.71%
4mod7-v1_96	164	496	485	0.12	3.31%
cnt3-5_179	175	842	517	0.59	48.73%
mod10_176	178	566	498	0.15	17.53%
4gt4-v0_80	179	596	504	0.11	22.06%
4gt12-v0_88	194	644	567	0.14	17.11%
0410184_169	211	877	664	0.61	31.98%
4_49_16	217	725	612	0.16	22.24%
4gt12-v1_89	228	751	669	0.19	15.68%
4gt4-v0_79	231	720	668	0.22	10.63%
hwb4_49	233	745	684	0.20	11.91%
4gt4-v0_78	235	739	683	0.19	11.11%
mod10_171	244	779	696	0.23	15.51%
4gt12-v0_87	247	786	714	0.21	13.36%
4gt12-v0_86	251	805	729	0.26	13.72%
4gt4-v0_72	258	818	741	0.27	13.75%
4gt4-v1_74	273	900	801	0.22	15.79%
mini-alu_167	288	919	836	0.24	13.15%
one-two-three-v0_97	290	861	853	0.23	1.40%
rd53_135	296	1029	919	0.36	15.01%
ham7_104	320	1123	979	0.30	17.93%
decod24-enable_126	338	1091	1005	0.30	11.42%
mod8-10_178	342	1228	1027	0.32	22.69%
4gt4-v0_73	395	1289	1153	0.43	15.21%
ex3_229	403	1247	1166	0.37	9.60%
mod8-10_177	440	1401	1299	0.46	10.61%
alu-v2_31	451	1458	1296	0.42	16.09%
C17_204	467	1588	1439	0.54	13.29%
rd53_131	469	1614	1394	0.52	19.21%
alu-v2_30	504	1627	1515	0.50	9.97%
mod5adder_127	555	1758	1576	0.60	15.13%
rd53_133	580	1954	1743	0.84	15.36%
majority_239	612	2073	1791	0.64	19.30%
ex2_227	631	2130	1895	0.73	15.68%
cm82a_208	650	2093	2020	0.93	5.06%
sf_276	778	2481	2241	0.74	14.09%
sf_274	781	2508	2275	0.87	13.49%
con1_216	954	3232	3040	1.50	8.43%
rd53_130	1043	3418	3110	1.39	12.97%
f2_232	1206	3887	3627	1.65	9.70%
rd53_251	1291	4435	3867	1.77	18.07%
hwb5_53	1336	4462	3942	1.52	16.63%
radd_250	3213	11330	10440	8.81	10.96%
rd73_252	5321	18670	17335	18.87	10.00%
cycle10_2_110	6050	21704	19699	25.44	12.81%
hwb6_56	6723	22502	20571	22.13	12.24%
cm85a_209	11414	41785	38616	72.29	10.43%

Circuit Name	Original Gates	Algorithm in [7]	Proposed Algorithm	Running Time(s)	Improvement
rd84_253	13658	50103	46284	115.99	10.48%
root_255	17159	61424	58297	204.43	7.06%
mlp4_245	18852	70980	63717	205.33	13.93%
urf2_277	20112	78710	70143	241.43	14.62%
sym9_148	21504	73234	67407	211.39	11.26%
hwb7_59	24379	82058	75605	240.25	11.19%
clip_206	33827	125443	115217	663.92	11.16%
sym9_193	34881	125917	117105	651.67	9.68%
dist_223	38046	137543	130271	829.44	7.31%
sao2_257	38577	145946	132533	989.69	12.49%
urf5_280	49829	183656	172758	1216.33	8.14%
urf1_278	54766	208475	196052	1666.36	8.08%
sym10_262	64283	235802	218264	2467.67	10.23%
Summarizing	485117	1769629	1636683	#	10.35%

Table 5: Comparison between our algorithm and the algorithm in [7] on IBM QX5, where ratio in the Comparison column is obtained by (added gates in our program) vs. (added gates in their program)

Circuit Name	Original Gates	Algorithm in [7]	Proposed Algorithm	Running Time(s)	Improvement
graycode6_47	5	5	5	0.00	0.00%
xor5_254	7	7	7	0.00	0.00%
ex1_226	7	7	7	0.00	0.00%
4gt11_84	18	18	18	0.00	0.00%
ex-1_166	19	19	19	0.00	0.00%
ham3_102	20	20	20	0.00	0.00%
4mod5-v0_20	20	29	20	0.00	90.00%
4mod5-v1_22	21	30	21	0.00	90.00%
mod5d1_63	22	22	22	0.00	0.00%
4gt11_83	23	35	23	0.00	92.31%
4gt11_82	27	39	30	0.00	69.23%
rd32-v0_66	34	34	34	0.00	0.00%
mod5mils_65	35	44	35	0.00	90.00%
4mod5-v0_19	35	44	35	0.00	90.00%
rd32-v1_68	36	36	36	0.00	0.00%
alu-v0_27	36	39	42	0.01	-75.00%
3_17_13	36	36	36	0.00	0.00%
4mod5-v1_24	36	48	36	0.00	92.31%
alu-v1_29	37	40	43	0.01	-75.00%
alu-v1_28	37	40	43	0.01	-75.00%
alu-v3_35	37	40	43	0.01	-75.00%
alu-v2_33	37	46	43	0.01	30.00%
alu-v4_37	37	40	43	0.01	-75.00%
miller_11	50	50	50	0.00	0.00%
decod24-v0_38	51	51	51	0.00	0.00%
alu-v3_34	52	55	58	0.01	-75.00%
decod24-v2_43	52	52	52	0.00	0.00%
mod5d2_64	53	65	65	0.01	0.00%
4gt13_92	66	84	66	0.00	94.74%
4gt13-v1_93	68	86	68	0.00	94.74%

Circuit Name	Original Gates	Algorithm in [7]	Proposed Algorithm	Running Time(s)	Improvement
one-two-three-v2_100	69	78	78	0.01	0.00%
4mod5-v1_23	69	81	78	0.02	23.08%
4mod5-v0_18	69	78	78	0.01	0.00%
one-two-three-v3_101	70	85	76	0.01	56.25%
4mod5-bdd_287	70	85	76	0.01	56.25%
decod24-bdd_294	73	94	88	0.02	27.27%
4gt5_75	83	98	98	0.02	0.00%
alu-v0_26	84	105	93	0.01	54.55%
rd32_270	84	102	96	0.01	31.58%
alu-bdd_288	84	129	108	0.03	45.65%
decod24-v1_41	85	103	100	0.02	15.79%
4gt5_76	91	118	106	0.02	42.86%
4gt13_91	103	109	118	0.02	-128.57%
4gt13_90	107	116	134	0.02	-180.00%
alu-v4_36	115	151	130	0.02	56.76%
4gt5_77	131	167	140	0.04	72.97%
one-two-three-v1_99	132	171	144	0.02	67.50%
rd53_138	132	171	159	0.05	30.00%
one-two-three-v0_98	146	173	170	0.04	10.71%
4gt10-v1_81	148	181	175	0.04	17.65%
decod24-v3_45	150	189	165	0.04	60.00%
aj-e11_165	151	175	169	0.02	24.00%
4mod7-v0_94	162	201	174	0.04	67.50%
alu-v2_32	163	202	178	0.02	60.00%
4mod7-v1_96	164	206	182	0.03	55.81%
cnt3-5_179	175	262	190	0.04	81.82%
mod10_176	178	214	202	0.03	32.43%
4gt4-v0_80	179	257	203	0.05	68.35%
4gt12-v0_88	194	215	215	0.05	0.00%
0410184_169	211	286	223	0.02	82.89%
4_49_16	217	286	253	0.04	47.14%
4gt12-v1_89	228	321	252	0.03	73.40%
4gt4-v0_79	231	327	243	0.04	86.60%
hwb4_49	233	278	266	0.04	26.09%
4gt4-v0_78	235	334	250	0.05	84.00%
mod10_171	244	304	268	0.04	59.02%
4gt12-v0_87	247	370	253	0.01	94.35%
4gt12-v0_86	251	374	260	0.02	91.94%
4gt4-v0_72	258	348	300	0.05	52.75%
4gt4-v1_74	273	387	351	0.10	31.30%
mini-alu_167	288	363	321	0.06	55.26%
one-two-three-v0_97	290	356	356	0.09	0.00%
rd53_135	296	344	350	0.11	-12.24%
ham7_104	320	422	401	0.08	20.39%
decod24-enable_126	338	419	425	0.14	-7.32%
mod8-10_178	342	504	363	0.04	86.50%
4gt4-v0_73	395	572	437	0.05	75.84%
ex3_229	403	577	421	0.05	89.14%
mod8-10_177	440	575	479	0.05	70.59%
alu-v2_31	451	514	505	0.07	14.06%
C17_204	467	581	563	0.14	15.65%

Circuit Name	Original Gates	Algorithm in [7]	Proposed Algorithm	Running Time(s)	Improvement
rd53_131	469	556	559	0.17	-3.41%
alu-v2_30	504	609	549	0.07	56.60%
mod5adder_127	555	642	606	0.11	40.91%
rd53_133	580	739	685	0.16	33.75%
majority_239	612	735	696	0.13	31.45%
ex2_227	631	901	727	0.22	64.21%
cm82a_208	650	872	734	0.14	61.88%
sf_276	778	1162	802	0.05	93.51%
sf_274	781	1162	805	0.04	93.46%
con1_216	954	1329	1146	0.39	48.67%
rd53_130	1043	1433	1214	0.31	56.01%
f2_232	1206	1431	1419	0.43	5.31%
rd53_251	1291	1600	1495	0.34	33.87%
hwb5_53	1336	1546	1510	0.30	17.06%
radd_250	3213	4860	3882	2.34	59.34%
rd73_252	5321	7436	6386	5.31	49.62%
cycle10_2_110	6050	8474	7346	6.25	46.52%
hwb6_56	6723	8442	7827	3.88	35.76%
cm85a_209	11414	15587	13751	16.67	43.99%
rd84_253	13658	18944	16904	37.18	38.59%
root_255	17159	22760	20684	48.44	37.06%
mlp4_245	18852	25314	22968	66.49	36.30%
urf2_277	20112	28317	26046	77.04	27.67%
sym9_148	21504	27942	23676	31.55	66.25%
hwb7_59	24379	30757	28981	63.92	27.84%
clip_206	33827	46451	40670	173.59	45.79%
sym9_193	34881	46335	41322	144.55	43.76%
dist_223	38046	50880	44982	187.64	45.95%
sao2_257	38577	50319	46404	233.36	33.34%
urf5_280	49829	70265	62894	374.76	36.07%
urf1_278	54766	79366	70444	649.03	36.27%
sym10_262	64283	84398	75980	518.75	41.85%
hwb8_113	24379	104756	84356	646.41	25.38%
Summarizing	509496	760639	670984	#	35.70%

Table 6: Comparison between our algorithm and the algorithm in [7] on IBM Q20, where ratio in the Comparison column is obtained by (added gates in our program) vs. (added gates in their program)

References

- [1] Gadi Aleksandrowicz, Thomas Alexander, P Barkoutsos, L Bello, Y Ben-Haim, D Bucher, FJ Cabrera-Hernández, J Carballo-Franquis, A Chen, CF Chen, et al. Qiskit: An open-source framework for quantum computing. *Accessed on: Mar, 16, 2019*.
- [2] Noga Alon, Fan RK Chung, and Ronald L Graham. Routing permutations on graphs via matchings. *SIAM journal on discrete mathematics*, 7(3):513–530, 1994.
- [3] Adriano Barenco, Charles H Bennett, Richard Cleve, David P DiVincenzo, Norman Margolus, Peter Shor, Tycho Sleator, John A Smolin, and Harald Weinfurter. Elementary gates for quantum computation. *Physical review A*, 52(5):3457, 1995.

- [4] Kyle EC Booth, Minh Do, J Christopher Beck, Eleanor Rieffel, Davide Venturelli, and Jeremy Frank. Comparing and integrating constraint programming and temporal planning for quantum circuit compilation. In *Twenty-Eighth International Conference on Automated Planning and Scheduling*, 2018.
- [5] Adi Botea, Akihiro Kishimoto, and Radu Marinescu. On the complexity of quantum circuit compilation. In *Eleventh Annual Symposium on Combinatorial Search*, 2018.
- [6] Andrew M Childs, Eddie Schoute, and Cem M Unsal. Circuit transformations for quantum architectures. *arXiv preprint arXiv:1902.09102*, 2019.
- [7] Alexander Cowtan, Silas Dilkes, Ross Duncan, Alexandre Krajenbrink, Will Simmons, and Seyon Sivaramajah. On the qubit routing problem. *arXiv preprint arXiv:1902.08091*, 2019.
- [8] Will Finigan, Michael Cubeddu, Thomas Lively, Johannes Flick, and Prineha Narang. Qubit allocation for noisy intermediate-scale quantum computers. *arXiv preprint arXiv:1810.08291*, 2018.
- [9] Thomas Häner, Damian S Steiger, Krysta Svore, and Matthias Troyer. A software methodology for compiling quantum programs. *Quantum Science and Technology*, 3(2):020501, 2018.
- [10] Toshinari Itoko, Rudy Raymond, Takashi Imamichi, Atsushi Matsuo, and Andrew W Cross. Quantum circuit compilers using gate commutation rules. In *Proceedings of the 24th Asia and South Pacific Design Automation Conference*, pages 191–196. ACM, 2019.
- [11] Scott Kirkpatrick, C Daniel Gelatt, and Mario P Vecchi. Optimization by simulated annealing. *science*, 220(4598):671–680, 1983.
- [12] Aleks Kissinger and Arianne Meijer-van de Griend. Cnot circuit extraction for topologically-constrained quantum memories. *arXiv preprint arXiv:1904.00633*, 2019.
- [13] Gushu Li, Yufei Ding, and Yuan Xie. Tackling the qubit mapping problem for nisq-era quantum devices. In *Proceedings of the Twenty-Fourth International Conference on Architectural Support for Programming Languages and Operating Systems*, pages 1001–1014. ACM, 2019.
- [14] Tillmann Miltzow, Lothar Narins, Yoshio Okamoto, Günter Rote, Antonis Thomas, and Takeaki Uno. Approximation and hardness for token swapping. *arXiv preprint arXiv:1602.05150*, 2016.
- [15] Prakash Murali, Jonathan M Baker, Ali Javadi-Abhari, Frederic T Chong, and Margaret Martonosi. Noise-adaptive compiler mappings for noisy intermediate-scale quantum computers. In *Proceedings of the Twenty-Fourth International Conference on Architectural Support for Programming Languages and Operating Systems*, pages 1015–1029. ACM, 2019.
- [16] Beatrice Nash, Vlad Gheorghiu, and Michele Mosca. Quantum circuit optimizations for nisq architectures. *arXiv preprint arXiv:1904.01972*, 2019.
- [17] Michael A Nielsen and Isaac L Chuang. Quantum information and quantum computation. *Cambridge: Cambridge University Press*, 2(8):23, 2000.
- [18] Shin Nishio, Yulu Pan, Takahiko Satoh, Hideharu Amano, and Rodney Van Meter. Extracting success from ibm’s 20-qubit machines using error-aware compilation. *arXiv preprint arXiv:1903.10963*, 2019.
- [19] Alexandru Paler. On the influence of initial qubit placement during nisq circuit compilation. In *International Workshop on Quantum Technology and Optimization Problems*, pages 207–217. Springer, 2019.
- [20] John Preskill. Quantum computing in the nisq era and beyond. *Quantum*, 2:79, 2018.
- [21] Marcos Yukio Siraichi, Vinícius Fernandes dos Santos, Sylvain Collange, and Fernando Magno Quintão Pereira. Qubit allocation. In *Proceedings of the 2018 International Symposium on Code Generation and Optimization*, pages 113–125. ACM, 2018.
- [22] Rodney Van Meter. *Quantum networking*. John Wiley & Sons, 2014.

- [23] Davide Venturelli, Minh Do, Eleanor G Rieffel, and Jeremy Frank. Temporal planning for compilation of quantum approximate optimization circuits. In *IJCAI*, pages 4440–4446, 2017.
- [24] Robert Wille, Austin Fowler, and Yehuda Naveh. Computer-aided design for quantum computation. In *2018 IEEE/ACM International Conference on Computer-Aided Design (ICCAD)*, pages 1–6. IEEE, 2018.
- [25] Alwin Zulehner, Alexandru Paler, and Robert Wille. An efficient methodology for mapping quantum circuits to the ibm qx architectures. *IEEE Transactions on Computer-Aided Design of Integrated Circuits and Systems*, 2018.